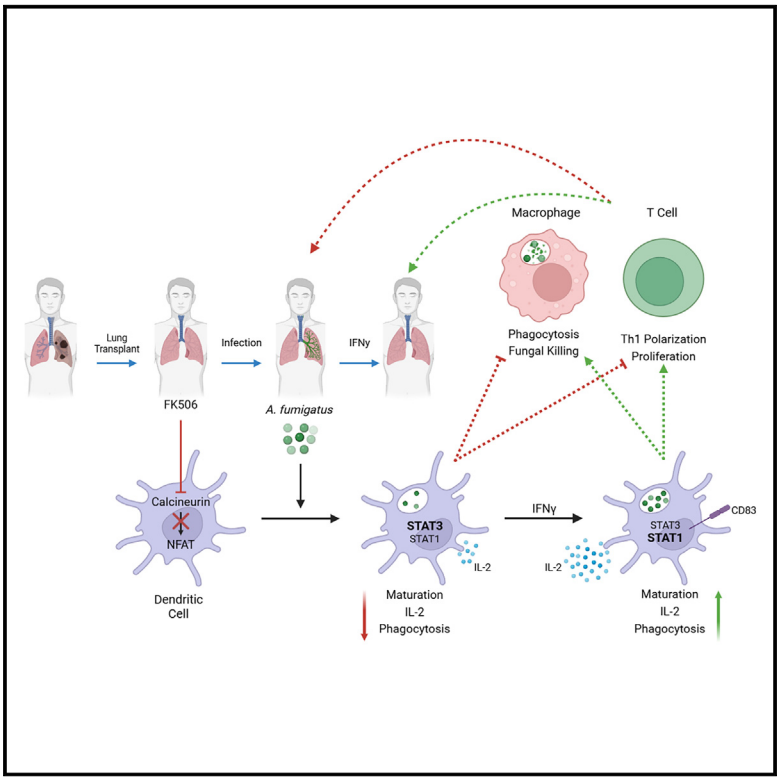
iScience

Article

Interferon-gamma rescues dendritic cell calcineurin-dependent responses to *Aspergillus fumigatus* via Stat3 to Stat1 switching

Graphical abstract



Authors

Amit Adlakha, Thomas J. Williams, Xinxin Shou, Anna K. Reed, Boris Lenhard, Darius Armstrong-James

Correspondence

d.armstrong@imperial.ac.uk

In brief

Pathophysiology; Microbiology; Transcriptomics

Highlights

- Calcineurin inhibitors block DC maturation in response to *A. fumigatus*
- Lack of DC maturation impairs Th1 polarization in response to *A. fumigatus*
- Interferon-γ restores maturation, promotes Th1 polarization and fungal killing
- ChIPseq reveals interferon-γ induces a regulatory switch from STAT3 to STAT1

Adlakha et al., 2025, iScience *28*, 111535
February 21, 2025 © 2024 Published by Elsevier Inc.
https://doi.org/10.1016/j.isci.2024.111535

CellPress

iScience

CellPress
OPEN ACCESS

Article

Interferon-gamma rescues dendritic cell calcineurin-dependent responses to *Aspergillus fumigatus* via Stat3 to Stat1 switching

Amit Adlakha,[1,2,3,4] Thomas J. Williams,[1,3,4] Xinxin Shou,[1] Anna K. Reed,[3] Boris Lenhard,[2] and Darius Armstrong-James[1,3,5,*]

[1]Department of Infectious Disease, Faculty of Medicine, Imperial College, London SW7 2AZ, UK
[2]MRC London Institute of Medical Sciences, Imperial College, London W12 0NN, UK
[3]Department of Cardiothoracic Transplantation and Mechanical Support, Harefield Hospital, Royal Brompton & Harefield Hospitals, Part of Guy's and St. Thomas' NHS Foundation Trust & Imperial College, London UB9 6JH, UK
[4]These authors contributed equally
[5]Lead contact
*Correspondence: d.armstrong@imperial.ac.uk
https://doi.org/10.1016/j.isci.2024.111535

SUMMARY

Invasive pulmonary aspergillosis is a lethal opportunistic fungal infection in transplant recipients receiving calcineurin inhibitors. We previously identified a role for the calcineurin pathway in innate immune responses to *A. fumigatus* and have used exogenous interferon-gamma successfully to treat aspergillosis in this setting. Here we show that calcineurin inhibitors block dendritic cell maturation in response to *A. fumigatus,* impairing the Th1 polarization of CD4 cells. Interferon gamma, an immunotherapeutic option for invasive aspergillosis, restored maturation and promoted Th1 polarization via a dendritic cell dependent effect that was co-dependent on T cell interaction. We find that interferon gamma activates alternative transcriptional pathways to calcineurin-NFAT for the augmentation of pathogen handling. Histone modification ChIP-Seq analysis revealed dominant control by an interferon gamma induced regulatory switch from STAT3 to STAT1 transcription factor binding underpinning these observations. These findings provide key insight into the mechanisms of immunotherapy in organ transplant recipients with invasive fungal diseases.

INTRODUCTION

Over 4000 lung transplant operations are performed worldwide annually.[1] Median survival for the 28,531 adults who underwent primary lung transplantation between 2009 and 2016 was 6.5 years, representing the poorest survival outcomes among the commonly transplanted solid organs. Infection remains the leading cause of death in the first year after lung transplantation as post-transplant immunosuppression renders the host susceptible to a broad range of pathogens, both obligate and opportunistic.[1] Lung transplant recipients have the highest rates of invasive aspergillosis of any transplant population, at 44%.[2] Invasive fungal infection in lung transplant recipients has the highest mortality rate across the organ groups with 58% after 2 years.[3,4]

Calcineurin inhibitors are the key class of maintenance immunosuppressive therapy in organ transplantation.[5] Tacrolimus (FK506) has emerged as the most frequently used calcineurin inhibitor, used by 83% of patients at one-year post-transplant.[6–8] Whilst calcineurin inhibitors demonstrate *in vitro* antifungal properties against *A. fumigatus*, its immunosuppressant activity counteracts any antimicrobial effect *in vivo*.[9]

A. fumigatus, when inhaled, is internalized by pulmonary dendritic cells (DC) and monocyte-derived DCs (moDC), which rapidly migrate to local lymph nodes whilst undergoing maturation, leading to the priming of $CD4^+$ T cells.[10] Immature DCs phagocytose *A. fumigatus*,[11] an act which reliably induces DC maturation.[12–14] Maturation of DCs has been shown to be accompanied by a switch from calcium ion oscillations to steady state concentrations.[15] Nuclear factor of activated T-cells, cytoplasmic 2 (NFATc2) protein production is rapidly induced by calcium influx in DCs[16] and hence the immature state is functionally similar to one of the nuclear factors of activated T-cells (NFAT) activity.[17] Stimulation leads to $Ca2^+$ mobilization by the engagement of CD14 and subsequent Src kinase activation, and this promotes calcineurin mediated NFAT dephosphorylation and translocation to the nucleus.[18]

Calcineurin itself has been investigated in DCs in response to whole pathogen and pathogen associated molecular pattern stimulation, including bacterial CpG nucleotides, Pam3CyS, Leishmania mexicana, Bacillus Calmette-Guerin (BCG) vaccine, and Escherichia coli, all of which trigger toll-like receptor (TLR)-dependent IL2 production.[19,20] Calcineurin inhibitors reduce the phosphatase activity of calcineurin and, in doing so, inhibit the nuclear translocation of the NFAT family of transcription factors (TF).[21] Our group has previously shown that in human alveolar macrophages, calcineurin/NFAT blockade via FK506 results in

This is an open access article under the CC BY-NC-ND license (http://creativecommons.org/licenses/by-nc-nd/4.0/).

Table 1. Demographic information of patients with lung transplant

	No Infection (n = 3)	Invasive *Aspergillus* Infection (n = 3)
Gender, *n* (%)		
Male	2 (66.7)	0 (0)
Female	1 (33.3)	3 (100)
Age (Years), Average ± SD	43 ± 7.5	43 ± 17.6
Indication, *n* (%)	–	–
Cystic Fibrosis	1 (33.3)	2 (66.7)
COPD	2 (66.7)	1 (33.3)
Transplant Type, *n* (%)	–	–
Double	3 (100)	3 (100)
Immunosuppression, *n* (%)	–	–
Prednisolone	3 (100)	3 (100)
Tacrolimus (FK506)	3 (100)	3 (100)
Mycophenolate mofetil (MMF)	3 (100)	3 (100)
Rejection On Biopsy	–	–
No	3 (100)	3 (100)
Yes	0 (0)	0 (0)
Aspergillus Positive BAL Culture, *n* (%)	–	–
No	3 (100)	0 (0)
Yes	0 (0)	3(100)
Antifungal Treatment, *n* (%)	–	–
No	3 (100)	3 (100)
Yes	0 (0)	0 (0)
Antifungal Prophylaxis, *n* (%)	–	–
No	2 (66.7)	3 (100)
Yes	1 (33.3)	0 (0)

impaired phagocytosis and fungal killing of *A. fumigatus*.[22,23] We discovered that calcineurin is activated via phagocytic signaling through TLR9 and Bruton's tyrosine kinase. In subsequent studies we observed that calcineurin drove necroptotic cell death responses that were crucial for control of infection via cell-to cell transfer through a process called metaforosis. In further studies, we have shown that transplant recipients with invasive fungal disease fail to mount appropriate interferon-gamma (IFNγ) responses, and we and others have shown the utility of exogenous IFNγ therapy in this setting.[24–26]

We therefore sought to understand the mechanistic basis for IFNγ -based "rescue" of fungal immunoparesis during transplant immunosuppression with calcineurin inhibitors, using dendritic cell-T cell interactions as a model. We show that monocyte-derived DC's are present in the transplanted lung during *A. fumigatus* infection, and that FK506 impairs moDC phagocytosis, an effect that is partially recovered by IFNγ treatment. We further reported that FK506 impairs moDC maturation in the context of *A. fumigatus* infection, though IFNγ treatment fully recovers the maturation status, perhaps accounting for the incomplete phagocytic recovery. We observed that in a mixed leukocyte reaction FK506 inhibits CD4 T cell stimulation by *A. fumigatus*-infected moDC's, and subsequent IFNγ treatment recovers this. We then show that CD4 cells cocultured with *A. fumigatus*-infected moDC's deviate from the Th1 phenotype in response to FK506 treatment, but subsequent IFNγ treatment repolarizes the phenotype toward Th1.

By comparative RNA Seq, we show that *A. fumigatus*-infected, FK506 treated moDCs, unlike MDMs, downregulate the NFAT target RCAN1 with IFNγ treatment during FK506 exposure, suggesting an NFAT-independent mechanism of fungal immunity in moDC's in this context. Genome-wide analysis of enhancer and promoter regions identified by ChIP-seq in dendritic cells that while enrichment of transcription factors known to be implicit in fungal immunity, such as NFATc2 and HIF1a, was seen across states, a significant switch from STAT3 to STAT1 enrichment was seen in the regulatory regions that became active on the IFNγ treatment of *A. fumigatus*, FK506-treated moDC's. Furthermore, we observed the reverse switch from STAT1 to STAT3, at regulatory regions that became inactive with IFNγ treatment. These findings suggest a key regulatory role for STAT1 in the moDC response to infection to *A. fumigatus* in the setting of chemical calcineurin-NFAT inhibition via an NFAT-independent mechanism.

RESULTS

FK506 impairs the function of monocyte-derived dendritic cells

We first assessed immune cell populations in bronchoalveolar lavage (BAL) fluid from patients with lung transplant either with no infectious pathology or with invasive aspergillosis. All patients had undergone a double lung transplant and showed no indications of allograft rejection. Patients were all on the same immunosuppression regimen of prednisolone, tacrolimus (FK506), and mycophenolate mofetil. Further demographic information is found in Table 1. BAL immune cells were enumerated by flow cytometry, and we observed that there was a significant increase in the number of dendritic cells (DC) in patients with aspergillosis compared to those without (Figure 1A). FK506 has previously been shown to impair the phagocytosis and fungal killing of *A. fumigatus* by alveolar macrophages,[22,23] therefore it is likely to also impact dendritic cells, which are essential to an effective immune response. As such, we sought to examine the effect of FK506 on *Aspergillus*-infected DCs *in vitro*.

Previous studies have highlighted that transplant recipients with invasive fungal disease fail to mount appropriate interferon-gamma (IFNγ) responses, and the utility of exogenous IFNγ therapy in this setting has been shown.[24–26] Therefore, alongside investigating the effect of FK506 on DCs *in vitro* we also aimed to examine whether the addition of IFNγ abrogates these effects. Monocyte-derived DCs (moDC) were treated with FK506 and/or IFNγ and infected with *A. fumigatus.* Treatment of cells with FK506 significantly reduced the number of DCs with internalized conidia after 30 min of infection, while IFNγ alone had no significant effect. Treatment of FK506-treated moDCs with IFNγ restored their phagocytic capacity (Figure 1B). Similarly, when examining the fungicidal capacity of moDCs by colony forming unit (CFU) assay, it was observed the treatment with FK506 or IFNγ alone significantly increased and decreased

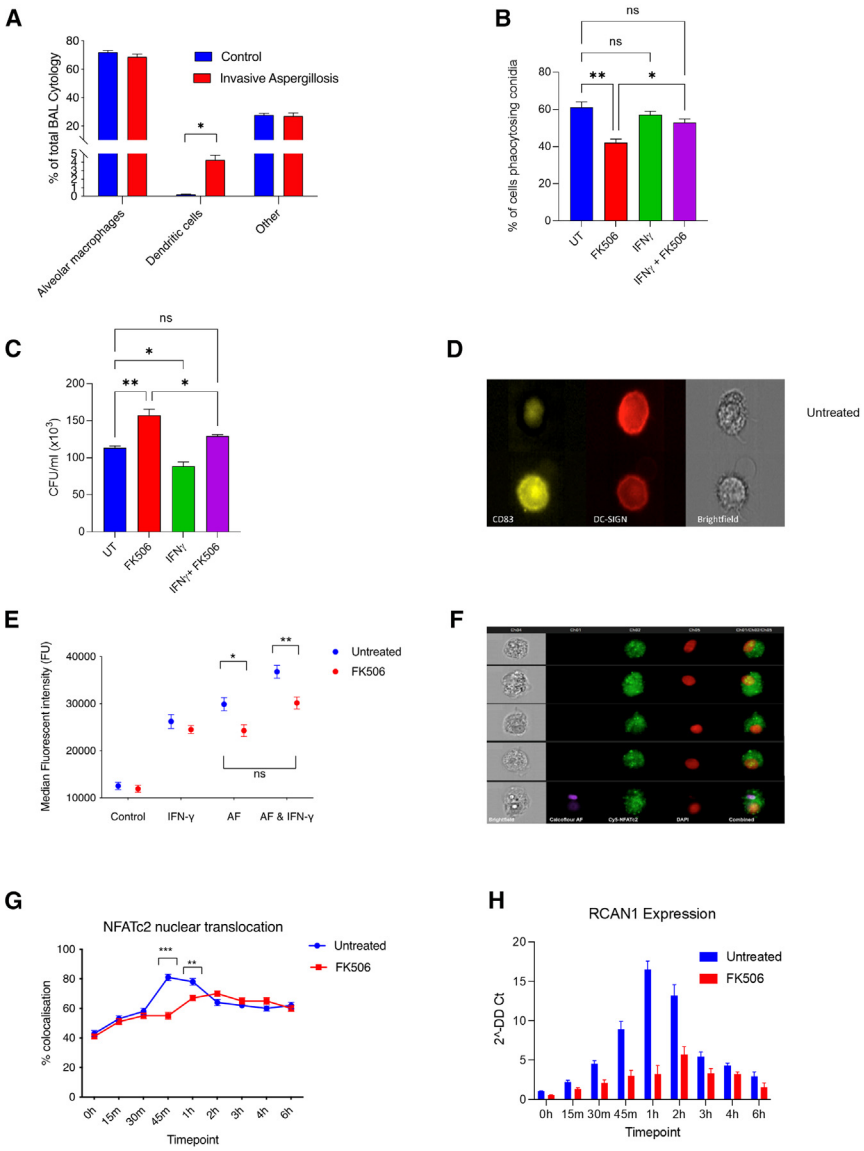


Figure 1. FK506 impairs the function of monocyte-derived Dendritic Cells

(A) Alveolar macrophage and dendritic cell populations in bronchoalveolar lavage of patients with lung transplant with and without invasive aspergillosis (n = 3).

(B) Phagocytosis of *A. fumigatus* conidia (MOI = 1) by dendritic cells untreated, treated with IFNy or FK506 or both for 30 min (n = 3).

(C) Fungal killing of *A. fumigatus* conidia (MOI = 1) by dendritic cells untreated, treated with IFNy or FK506 or both 6 h post infection, measured by CFUs (n = 3).

(D) Representative ImageStream images of CD83 on moDCs treated with or without IFNy.

(E) MFI of CD83 on moDCs untreated, treated with IFNy and/or FK506, infected with *A. fumigatus* (MOI = 1) or uninfected (n = 3).

(F) Representative ImageStream images of moDCs stained for nucleus (DAPI) and NFATc2 (Cy5), and infected with *A. fumigatus* (MOI = 1) or uninfected (n = 3).

(G) Timecourse of NFATc2 nuclear translocation of *A. fumigatus* infected (MOI = 1) moDCs treated with and without FK506 (n = 3).

(H) Time course RCAN-1 expression of *Aspergillus* infected (MOI = 1) moDCs DCs treated with and without FK506 (n = 3). $^{*}p < 0.05$; $^{**}p < 0.01$; $^{***}p < 0.001$ (A) t-test (B, C, E, and H) one-way ANOVA (G) two-way ANOVA. Data represented as mean ± SEM.

numbers of CFUs respectively. Lastly, moDCs that were treated with both FK506 and IFNγ showed a similar level of fungal killing to the untreated control (Figure 1C).

We next assessed how these treatments affect DC maturation, by measuring CD83 expression (Figure 1D). MoDCs treated with FK506 and infected with *A. fumigatus* had significantly lower expression levels of CD83 compared to untreated infected controls, which was rescued by treatment with IFNγ (Figure 1E).

Imagestream analysis revealed that FK506 treatment significantly reduced NFAT nuclear translocation in infected DCs during the first hour post-infection compared to untreated controls (Figures 1F and 1G). A similar effect was seen via PCR for expression of the NFAT-dependant signaling inhibitor RCAN1 which again was significantly reduced in FK506 treated cells (Figure 1H).

These data suggests that FK506 acts as an inhibitor of DC maturation and impairs their ability to phagocytose and kill *A. fumigatus* conidia. Furthermore, IFNγ therapy may be used to restore DC function.

FK506 treatment abrogates T cell activation by dendritic cells

DCs are professional antigen-presenting cells that play a key role in the initiation of an immune response through the interaction and activation of other immune cells, primarily T cells. Therefore, we next investigated how FK506 and IFNγ treatment of moDCs modulated T cell proliferation and maturation during *A. fumigatus* infection in DC/T cell co-cultures. To do this, moDCs were treated with FK506, IFNγ or both, washed and co-incubated with T cells for 12 h. Both IFNγ and *A. fumigatus* alone increased T cell proliferation compared to untreated controls, with the later having the more profound effect, whereas FK506 reduced proliferation and expression of CXCR3, marker used to differentiate effector and memory T cells from naive (Figures 2A and 2B).

Within the environment of the lung the primary antigen-presenting cells are alveolar macrophages. Macrophages, such as DCs play an essential role in the activation and polarization of the T cell response. As previous studies have shown FK506-dependent impairment of alveolar macrophage function,[22,23] and knowing that the FK506 treatment of moDCs altered the maturation of T cells, we next investigated the impact of FK506

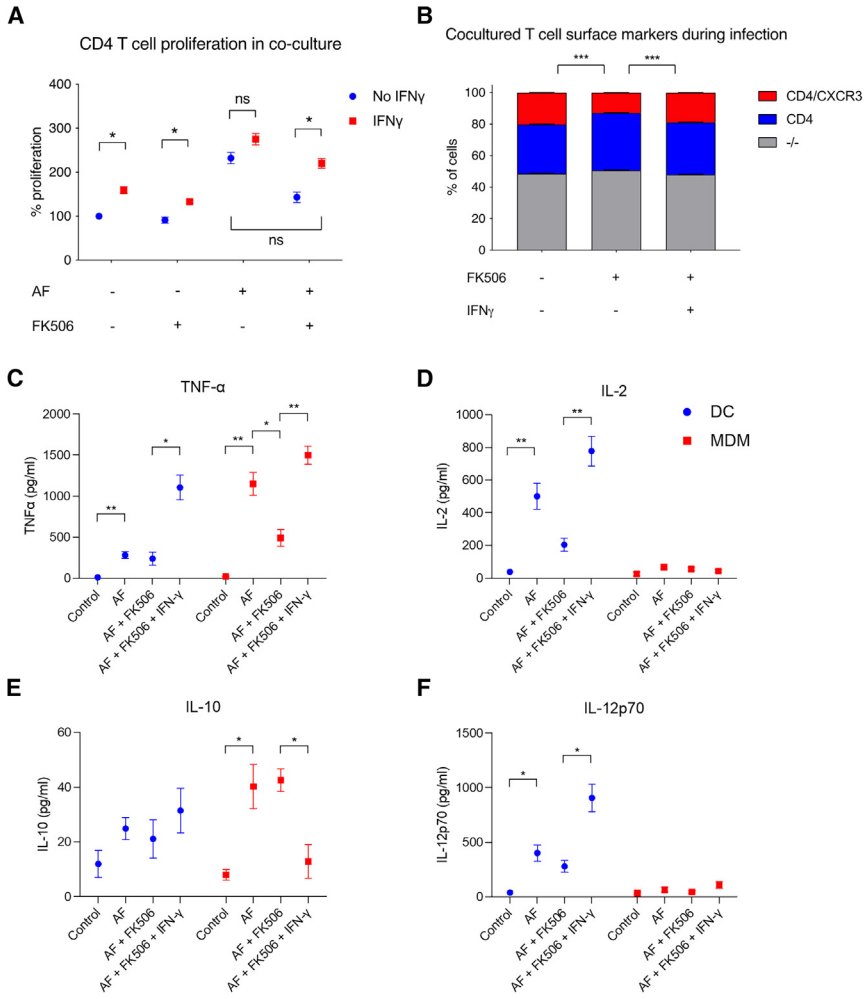


Figure 2. FK506 treatment abrogates T cell activation by Dendritic Cells

(A) CD4 cell proliferative capacity measured in a mixed leukocyte reaction of T cells and moDC's, with *A. fumigatus* infection (MOI = 1), FK506 and IFN-γ treatment ($n = 3$).

(B) CXCR3 surface expression on CD4 T cells co-cultured with moDC's with *A. fumigatus* infection (MOI = 1), FK506 and IFN-γ treatment.

(C and D) Cytokine secretion by moDCs or MDMs with *A. fumigatus* infection (MOI = 1), FK506 and IFN-γ treatment ($n = 3$), (C) TNFa, (D) IL-2, (E) IL-10 and (F) IL-12. $^{*}p < 0.05$; $^{**}p < 0.01$; $^{***}p < 0.001$ (A–F) one-way ANOVA. Data represented as mean ± SEM.

on the secretion of polarizing cytokines, including Tumor Necrosis Factor (TNF)α, Interleukin (IL)-2, IL-10 and IL-12, from both moDCs and monocyte-derived macrophages (MDM) for comparison of primary lung phagocytes. FK506 treatment led to decreased TNFα secretion by MDMs during *A. fumigatus* infection, although not by moDCs, an effect which is abrogated by IFNγ stimulation (Figure 2C). In contrast, FK506 reduced IL-2 secretion by moDCs during *A. fumigatus* infection, which was similarly rescued by IFNγ (Figure 2D). IL-10 and IL-12 secretion by moDCs or MDMs were not altered by FK506 treatment, however IFNγ was able to induce moDC IL-12 and MDM IL-10 during infection in the presence of FK506 (Figures 2E and 2F).

These findings support the conclusion that IFNγ treatment, rather than directly influencing macrophage phagocytosis, reverses the FK506-mediated abrogation of T cell activation capacity of DCs.

FK506 treatment alters the transcriptome of both dendritic cells and macrophages

To dissect the pathways underpinning these observations RNA-seq analysis was carried out on the primary phagocytes of the lung, DCs and MDMs, at 1 h post infection to identify and compare transcriptomes when treated with FK506 or IFNγ individually or in combination.

Complete linkage clustering of the top 200 genes with the greatest inter-condition variance revealed profound clustering for cell type, treatment, and infection. Genesets were separated into 5 broad hierarchically defined clusters. Clusters 1 and 4 represented genes preferentially up- and downregulated respectively in non-INFγ treated moDCs. Cluster 2 represented genes preferentially upregulated in non-IFNγ treated MDMs. Clusters 3 and 5 represented preferentially up- and downregulated genes respectively with IFNγ treatment irrespective of cell type (Figure 3A).

Infection with *A. fumigatus* of moDCs and MDMs led to differential expression of 12 and 96 genes respectively, compared to uninfected controls (Tables S1 and S12). moDCs and MDMs have distinct transcriptional response to *Aspergillus fumigatus* with an overlap of only 2 genes, CCL3L3 and TNFα, both of which demonstrated significantly higher expression in MDMs than in moDCs (Figure 3B).

We next examined how FK506 treatment alters these transcriptional responses. For moDCs only 5 genes were found to be differentially expressed, with 4 upregulated genes including CCR3, and 1 downregulated gene, SEPP1 (Table 2). Similarly, FK506 treatment showed a modest differential expression profile for MDMs with only 4 downregulated genes. These include RCAN1, EGR3 and NR4A2, and BAMBI (Table 2).

We next sought to establish how IFNγ affects the transcriptomic response to *A. fumigatus* in both moDCs and MDMs. We observed a greater number of differentially expressed genes in IFNγ treated uninfected moDCs compared to infected cells, and the reverse for MDMs (Figure 4A) (Tables S3 and S4). Gene ontology highlighted a tendency for IFNγ treatment to influence biochemical, structural and T cell stimulatory processes in both uninfected moDCs and MDMs (Figures 4B and 4C).

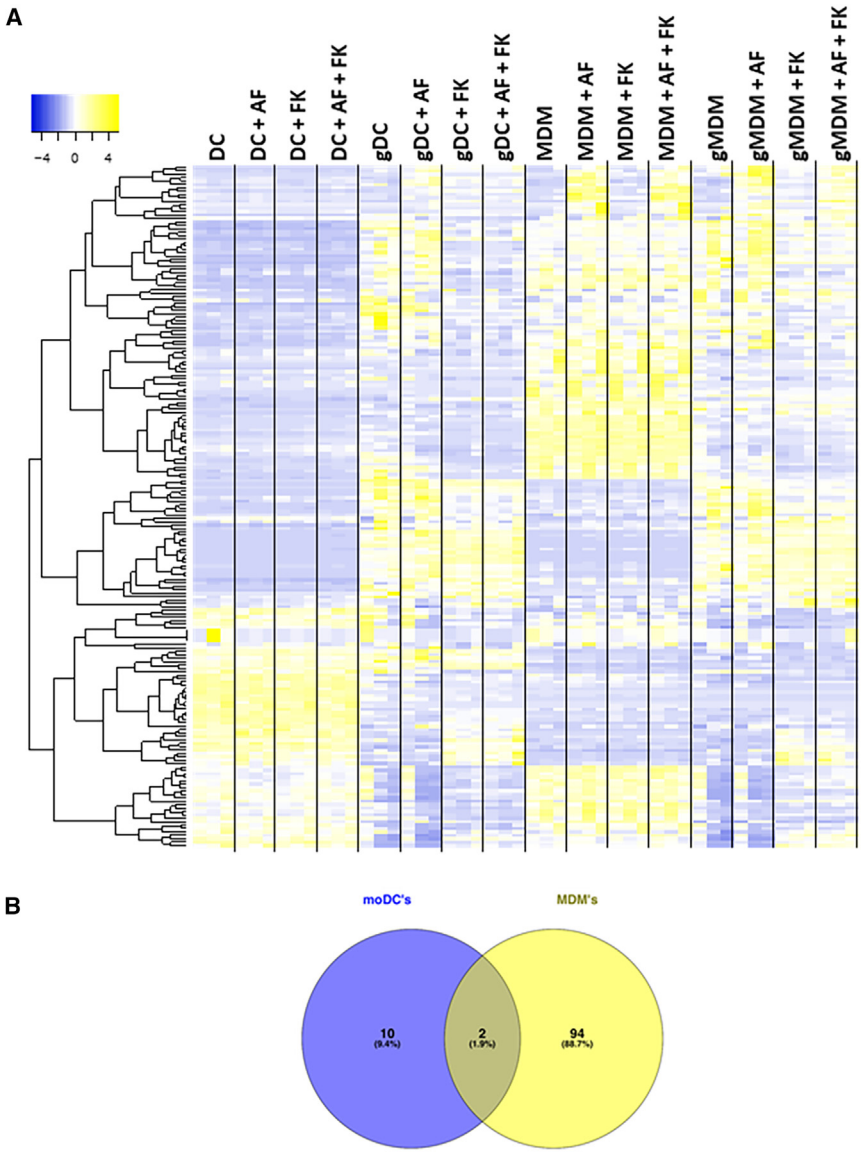


Figure 3. IFNγ and FK506 treatment alters the transcriptomic response to *A. fumigatus* in both moDCs and MDMs

MoDC's and MDM's from healthy volunteers ($n = 3$) were pre-treated with FK506 and/or IFNγ, then infected with *A. fumigatus* (MOI = 1) for 1 h prior to sequencing (A) Gene expression heatmap of top 200 genes (ranked by SD) per unclustered condition.

(B) Venn diagram showing overlap of differentially expressed genes in infected moDCs and MDMs.

Infection with *A. fumigatus* of IFNγ treated moDCs led to differential expression of 6 genes when compared to uninfected controls, an effect not seen in MDMs, suggesting an *A. fumigatus* infection induced transcriptomic effect specific to moDCs (Table S5).

We next examined the IFNγ-specific effect on FK506 treatment in infected moDCs and MDMs. FK506 treatment led to a large expansion in the numbers of differentially expressed genes in infected IFNγ treated moDCs and MDMs (Figure 4D) (Table 3).

For FK506 treated infected MDMs, IFNγ had the effect of upregulating FosB, a component of NFAT's co-transcription factor AP-1, suggesting NFAT activity in MDMs. Having previously observed the upregulation of RCAN1 with IFNγ treatment in infected moDCs, suggesting augmented chromatin-binding of NFAT, we unexpectedly found that IFNγ facilitates significant suppression of RCAN1 with FK506 treatment of infected cells. This phenomenon was not observed with FK506 treatment alone of infected cells, thus it appears to be a specific IFNγ effect that is dependent on FK506 activity. This finding raises the possibility that the favourable antifungal phenotypic effects of IFNγ on FK506-treated moDCs seen previously are not directly via NFAT. Such an effect with IFNγ on RCAN1 was not observed in MDMs.

The epigenetic landscape in the moDC response to infection and interferon gamma reveals differential control in three key pathways: NFAT, HIF1a and STAT, but with dominant control of STAT3 to STAT1 during IFNγ treatment.

Gene transcription occurs in an epigenetic landscape that remodels to selectively permit transcription factor-chromatin interaction.[27] This is closely followed by chromosomal looping that permits direct chromatin contact between promoter and enhancer sites, thereby initiating gene transcription.[28] Thus, analysis of epigenetic modifications that facilitate open and active chromatin at regulatory regions may reveal transcription factors with crucial roles in initiating gene transcription during *A. fumigatus* infection and FK506 treatment.

Having observed differential transcriptomic responses, we used histone modification ChIP-Seq to explore the control of gene regulation in moDCs in response to *A. fumigatus*. Infection of moDCs with *A. fumigatus* led to a differential binding of anti-histone 3 lysine 27 acetylation (H3K27ac) at 901 genome-wide sites. At 435 sites, there was significantly increased binding with infection, with a corresponding decrease at 466 sites (Figures 5A and 5B).

Topologically associating domains (TAD) of genes that were differentially expressed with *A. fumigatus* infection were then isolated, and there was significantly more differential H3K27ac signal in these regions (Figure 5C), specifically around a subset of 8 of the 12 differentially expressed genes – TNF, MUC2, CCL3L3, NGFR, CLEC4D, ZFPM2, EVA1C and TMEM182.

Table 2. All genes differentially expressed with the FK506 treatment of *A. fumigatus* infected moDC's and MDMs

Cell	Ensembl Gene ID	HGNC symbol	Log FC	FDR *p*-value
moDCs	ENSG00000165152	TMEM246	6.32	0.012
	ENSG00000069188	SDK2	3.15	0.018
	ENSG00000250722	SEPP1	−5.75	0.039
	ENSG00000175920	DOK7	5.56	0.043
	ENSG00000183625	CCR3	5.68	0.043
MDMs	ENSG00000159200	RCAN1	−4.33	3.39E-20
	ENSG00000179388	EGR3	−3.23	7.03E-05
	ENSG00000095739	BAMBI	−2.32	1.87E-03
	ENSG00000153234	NR4A2	−2.27	9.24E-03

When *A. fumigatus* FK506-treated moDCs were subsequently treated with IFNγ, this led to the differential binding of anti-H3K27ac at 1335 genome-wide sites, with 822 and 513 sites of increased and decreased binding respectively (Figures 5D and 5E). In terms of upregulated regions, there was predominant enrichment of HIF1A and NFATC2, along with AP-1 and NFKB motifs (Table S6) and STAT1, BATF, IRF1, IRF2 and c-Fos TF binding sites (TFBS) (Table S7). Interestingly, when looking at downregulated H3K27ac regions genome-wide, NFATC2 and HIF1A were again enriched, and thus their influence on gene regulation in this context is not clear, possibly pointing toward different subsets of moDCs that respond differently in these conditions. Over-representation analysis of increased and decreased anti-H3K27ac-bound regions in TADs of upregulated and downregulated genes respectively revealed similar TF motifs and binding sites to that observed with the relevant genome-wide comparison. This suggests that TF control at differentially expressed genes is broadly representative of a genome-wide state, but also raises the possibility of significant gene expression that was not captured by the RNA-Seq timescale (Figure 5F).

With IFNγ treatment of infected, FK506-treated moDC's, NFATc2 was the top immune TF, and c-Fos and STAT3 predominated the TFBS database interrogation. Thus, whilst NFATc2 signal is seen both at regions of increased and decreased H3K27ac signal in TADs of upregulated genes, STAT3 was only seen in decreased regions, pointing toward a mechanism of STAT3 depletion in the IFNγ response in this context.

Interferon-gamma, but not A. fumigatus infection, significantly alters the moDC promoter and enhancer landscape, whereas both modify activity of these regulatory regions.

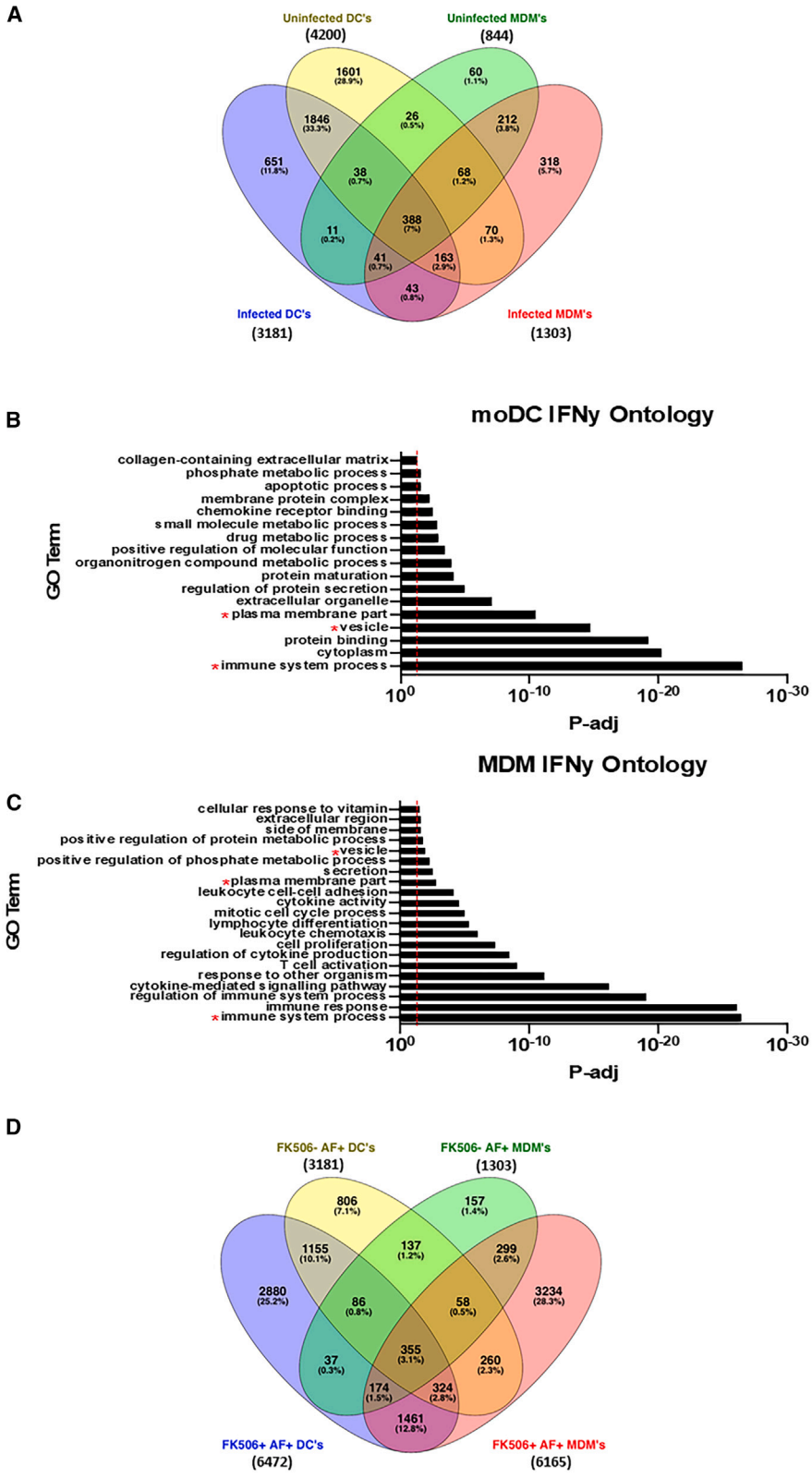
No conditional changes in genome-wide Histone 3 lysine 4 trimethylation (H3K4me3) distribution were observed between condition and control with *A. fumigatus* infection or FK506 treatment of moDC's. However, IFNγ treatment of resting moDCs induced changes in H3K4me3 signal at 1044 regions, of which the majority were increased signal (848 occurrences). The effect of IFNγ treatment on infected, FK506-treated moDCs was also profound, leading to 715 differentially bound H3K4me3, with an increase in binding at 651 sites. Whilst there was no significant infection-induced H3K4me3 signal, it was still possible to examine differential activity at promoters with greater resolution by examining differential H3K27ac signal at H3K4me3 marked regions. These common H3K4me3 peaks were overlapped with the 430 regions of increased H3K27ac binding with infection, to give 120 regions where promoters therefore gained activity with infection. Over-representation analysis at these sites notably showed enrichment of NFATc2, NFKB, HIF1a, and STAT3 (Tables S8 and S9). The same overlap analysis was carried out to determine the effect of IFNγ on *A. fumigatus* infected FK506 treat moDCs. This showed enrichment of NFATC2 and co-bound TFs where H3K27ac was both increased (Table S10) and decreased with IFNγ treatment. Conversely, STAT1 enrichment was only observed at regions of increased H3K27ac binding (Table S11) and STAT3 only with reduced H3K27ac binding, supporting a regulatory STAT3 to STAT1 switch during the IFNγ treatment of *A. fumigatus* infected, FK506-treated moDCs.

Turning to enhancers, a similar imbalance of effect of IFNγ vs. either *A. fumigatus* infection or FK506 treatment on the genomic distribution of histone 3 lysine 4 monomethylation (H3K4me1) signal was seen, the latter two producing <10 differentially bound anti-H3K4me1 sites genome-wide. In contrast, IFNγ treatment of resting moDCs induced changes in H3K4me1 signal at 891 regions. An increased H3K4me1 signal was observed at a majority of the regions (836 occurrences), suggesting that IFNγ pervasively promotes the emergence of enhancers from a state of latency. Looking at the effect of IFNγ treatment on infected FK506-treated moDCs there were 715 differentially bound H3K4me1 sites, with an increase in binding at 651 sites.

Analysis for differential H3K4me1 binding with the IFNγ treatment of infected, FK506-treated moDCs notably revealed a limited TFBS list, all of which suggested STAT1 binding at these sites (Table S12). As above, differential activity at enhancers was investigated by examining differential H3K27ac signal at H3K4me1 marked regions. Over-representation analysis at these sites notably showed the enrichment of NFATc2 and HIF1a motifs (as well as NR4A2, AP1, NFKB, Egr1 and Stat3) (Table S13) and predominantly NFKB, Fos, Jun and STAT3 TFBSs (Table 14). Examination of the IFNγ effect revealed regions of differential H3K27ac at H3K4me1-defined enhancers showed the enrichment of NFATC2 and co-bound TFs where H3K27ac was both increased (Table S15) and decreased with IFNγ treatment. Conversely, STAT1 enrichment was only observed at enhancers with increased H3K27ac binding (Table S16) and STAT3 enrichment only where there was reduced H3K27ac binding, this was also observed at regions of differential H3K27ac signal in TADs of differentially expressed genes. These results, showing a STAT3 to STAT1 switch with IFNγ treatment at both enhancer and promoter regions, imply a key advantageous role for STAT1, or more specifically, the switch from STAT3 to STAT1 activity in the DC response to *A. fumigatus* in the setting of calcineurin inhibition.

DISCUSSION

Invasive aspergillosis is a life-threatening complication of organ transplantation, in part due to the effects of calcineurin inhibition on innate immune responses to *Aspergillus fumigatus*. Whilst IFNγ has been used successfully in clinical practice as salvage



(legend on next page)

therapy in this context, as well as for invasive candidiasis and cryptococcal meningitis, the mechanistic basis for immunotherapeutic rescue in this setting has not been studied. Given the central role that dendritic cells play in coordinating immunological responses, we sought to characterize their role further in this context.

We found that CD1c positive dendritic cells are present in the alveolar compartment of lung transplant recipients, albeit in low numbers, and that overall numbers increase during *Aspergillus* infection, presumably due to the pulmonary recruitment of circulating moDCs. This is in keeping with clinical studies on human lung graft recipients demonstrating that recipient circulating monocytes are able to seed the alveoli early after transplantation and thus contribute to the repopulation of the alveolar macrophage compartment.[29]

We observed that the calcineurin inhibitor FK506 (Tacrolimus) impaired phagocytosis of *Aspergillus fumigatus* by human monocyte-derived dendritic cells, reducing CD83 (a late maturation marker) expression and IL-2 secretion. Treatment of dendritic cells with FK506 led to reduced expression of CXCR3 and subsequent reduced the proliferation of T cells in DC-T cell co-cultures. Furthermore, IFNγ rescue reversed these defects restoring phagocytic capacity, CD83 and IL-2 secretion. In addition, IFNγ augmented IL-12 expression in moDCs and rescued the T cell proliferation of and CXCR3 expression in moDC-T cell co-culture. These observations are indicative of a model where IFNγ treatment reverses the FK506-mediated abrogation of T cell activating capacity of DCs, and in doing so, indirectly promotes MDM phagocytosis.

To better understand the regulatory pathways underlying these observations, RNA-seq analysis in moDCs and MDMs was performed during *Aspergillus* infection. This analysis revealed that whilst the impact of FK506 on both moDC and MDM transcriptional responses to *A. fumigatus* was modest, FK506 had a dominant effect on moDC transcriptome when compared to MDMs. However, when moDCs or MDMs were treated with IFNγ, the impact of FK506 on transcriptional responses was much more pronounced, identifying core functional interplay between the calcineurin and IFNγ regulatory pathways.

Further examination of the gene sets involved indicated that the effects of IFNγ

were independent of NFAT. To better define the key pathways responsible for these complex observations, we undertook histone modification ChIP-seq to characterize the epigenetic landscape during *Aspergillus* infection.

Our analysis showed the predominant representation of the HIF1a transcription factor in the moDC response to *A. fumigatus* infection, with NFATc2/AP1/NFKB and STAT3 also present. The involvement of the NFAT pathway in the moDC response to *A. fumigatus* is well described. However, the finding of HIF1a as the top represented motif at active chromatin sites genome-wide is noteworthy. While multifaceted in its effects, HIF1a has a established role in anti-fungal immunity, via decreased production of chemokines and myeloid-cell dependent induction of aberrant neutrophil apoptosis, though is not required for conidial killing by phagocytes.[30] Cross-talk between NF-κB (downstream of dectin-1 binding) and HIF1a mediates the DC response against infection.[31] Furthermore, calcineurin inhibits the ubiquitination and proteasomal degradation of HIF1a via inhibition of the dimerization of the RACK1 scaffold protein, thereby promoting HIF1a degradation.[32] This finding indicates a protein-level, NFAT-independent mechanism by which calcineurin inhibitors could impair the moDC response to *A. fumigatus*. We further observed broad effects for IFNγ during *A. fumigatus* infection, however in the context of FK506 suppression combined H3K27ac, H3K4me3 and H3K4me1 ChIP-seq identified specific enrichment of HIF1a, NFATc2, NFKB, and STAT3, with evidence for IFNγ -dependent switching from STAT3 to STAT1 at active regulatory regions.

The finding that *A. fumigatus* profoundly alters the H3K27ac signal both genome-wide and more so in TADs around corresponding differentially expressed genes arises the possibility that the dendritic cell response to *A. fumigatus* infection is modulated at the level of chromatin. The interaction of pathogen and host cells that culminates in the modification of the host immune transcriptional response via epigenetic mechanisms is well-described with bacterial pathogens.[33] Epigenetic modifications, in particular in histone acetylation[34,35] can support pro-inflammatory phenotype change to support pathogen clearance.[36] We saw no differential H3K4me3 signal in moDC's with infection, with H3K4me3 present in both the control and infected state. This may suggest a pre-active "poised" state for promoters in moDC's which may well be differentiation state dependent, and that the activation of the promoter is only revealed by a differential H3K27ac signal, as was seen above. Consistent with this, and our findings of widespread changes in H3K4me1 signal, Mycobacterium tuberculosis was shown to only rarely induce de-methylation and gain of histone activation marks at promoter regions, instead these signals were enriched at distal enhancer elements.[37]

Taken together these observations identify widespread effects of FK506 on NFAT-dependent transcriptional and functional responses in moDCs. Notably, the effects of IFNγ on moDCs is much more pronounced in the context of FK506 immunosuppression, and sufficient to influence both subsequent T cell and MDM responses during infection. Epigenetic analysis identified STAT-3 to STAT-1 switching as a core effect of IFNγ in this setting. This is particularly interesting, as individuals with STAT3 mutations are prone to respiratory bacterial and fungal infections, including with *A. fumigatus*, and individuals with STAT1 mutations are prone to chronic mucocutaneous candidiasis.[38] Our observations are consistent with previous studies, which identify the activation of JAK1, JAK2 and STAT1 as key biological effects of IFNγ.[39] Taken together, these observations further reinforce the functional importance of STAT signaling for fungal immunity and demonstrate that exogenous IFNγ therapy is sufficient to rescue the knock-on effects of defective innate

Figure 4. Effects of IFNγ on moDC and MDM transcriptional responses during *A. fumigatus* infection

(A) Numbers of differentially expressed genes with IFNγ treatment in moDC's and MDM's, with and without *A. fumigatus* infection.

(B and C) Gene ontology of upregulated genes with IFNγ treatment in (B) moDCs and (C) MDMs.

(D) Number of differentially expressed genes in infected cells with IFNγ treatment, with and without FK506 treatment.

Table 3. All genes differentially expressed by IFNγ treatment during the FK506 treatment of infected moDC's and MDMs

Cell	Ensembl Gene ID	HGNC symbol	Log FC	FDR *p*-value
moDCs	ENSG00000159335	PTMS	3.12	5.00E-04
	ENSG00000256618	MTRNR2L1	−5.98	2.20E-03
	ENSG00000181222	POLR2A	2.62	4.90E-03
	ENSG00000159200	RCAN1	−2.72	6.50E-03
	ENSG00000177732	SOX12	3.42	0.013
	ENSG00000148773	MKI67	5.4	0.016
	ENSG00000047597	XK	5.58	0.019
	ENSG00000141867	BRD4	2.23	0.024
	ENSG00000121053	EPX	5.62	0.026
	ENSG00000101670	LIPG	−5.42	0.033
	ENSG00000167182	SP2	2.21	0.039
	ENSG00000005075	POLR2J	2.22	0.039
	ENSG00000117724	CENPF	4.14	0.039
	ENSG00000118181	RPS25	2.06	0.040
	ENSG00000132510	KDM6B	2.6	0.041
	ENSG00000168754	FAM178B	5.86	0.045
	ENSG00000170004	CHD3	2.18	0.047
MDMs	ENSG00000188886	ASTL	4.94	5.86E-05
	ENSG00000130518	IQCN	5.08	3.00E-04
	ENSG0000012 5740	FOSB	4.06	5.00E-04
	ENSG00000065621	GSTO2	4.48	6.00E-04
	ENSG00000173212	MAB21L3	4.44	7.00E-04
	ENSG00000260898	ADPGK-AS1	3.38	1.80E-03
	ENSG00000105290	APLP1	4.32	3.50E-03
	ENSG00000105939	ZC3HAV1	2.24	3.60E-03
	ENSG00000239653	PSMD6-AS2	3.4	3.70E-03
	ENSG00000229719	MIR194-2HG	5	3.70E-03
	ENSG00000253506	NACA2	−2.74	0.012
	ENSG00000126259	KIRREL2	5.2	0.012
	ENSG00000119737	GPR75	3.66	0.014
	ENSG00000173976	RAX2	4.5	0.014
	ENSG00000267270	PARD6G-AS1	3.58	0.020
	ENSG00000178184	PARD6G	3.25	0.026
	ENSG00000113916	BCL6	2.04	0.042
	ENSG00000129194	SOX15	3.76	0.048

calcineurin signaling in organ transplantation via STAT1 activation. Further studies are required to confirm these interactions in organ transplant recipients with invasive fungal infections receiving IFNγ immunotherapy.

Limitations of the study

In this study we have used monocyte derived DCs to investigate how FK506 negatively impacts the DC response to A. fumigatus and how IFNγ rescues this phenotype. It is important to mention that one can get nearly 100,000 DCs in good condition from bronchoalveolar lavage, using magnetic bead-based kits. Therefore, using primary DCs is a major limitation for high-throughput genomic analysis such bulk RNA-seq and ChIP-seq that we reported here. Future studies should implement single cell sequencing approaches, which requires fewer cells, to validate these finding using primary lung DCs.

RESOURCE AVAILABILITY

Lead contact

Further information and requests for resources and reagents should be directed to and will be fulfilled by the lead contact, Darius Armstrong-James (d.armstrong@imperial.ac.uk).

Materials availability

This study did not generate new unique reagents.

Data and code availability

- Data - The RNA-seq and ChIP-Seq datasets generated during this study are available at NCBI Sequence Read Archive: PRJNA1053273.

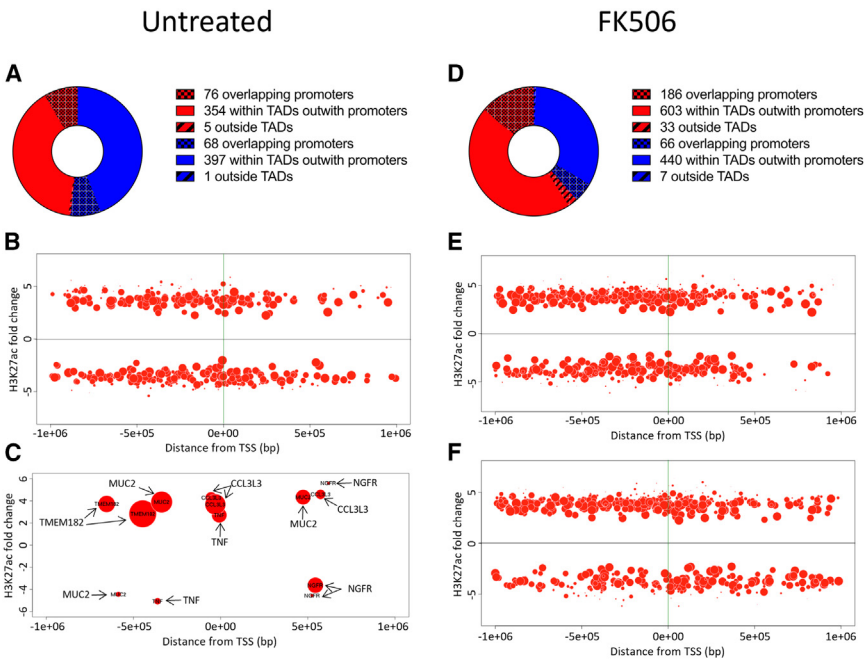


Figure 5. FK506 and IFNy treatment alter the epigenetic landscape of *A. fumigatus* infected DCs

(A) Sites of differential H3K27ac binding with the *A. fumigatus* infection of untreated moDC's.

(B and C) Genome-wide distribution of differential H3K27ac signal around nearest gene transcription start site (TSS, green line) with the *A. fumigatus* infection of untreated moDCs.

(D) Sites of differential H3K27ac binding with the IFN-γ treatment of *A. fumigatus* infected FK506-treated moDCs.

(E and F) Genome-wide distribution of differential H3K27ac signal with respect to nearest gene transcription start site (TSS, green line) with the IFN-γ treatment of *A. fumigatus*, FK506-treated moDCs.

- Code – All data were analyzed using publicly available packages as described in "method details"
- Other items – Any additional information required to reanalyze the data reported in this article is available from the lead contact upon request

ACKNOWLEDGMENTS

This work was funded by the MRC Chain-Florey Clinical Research Fellowship Scheme (to AA) D.A-J. holds funding from; Wellcome Trust (no. 219551/Z/19/Z), Medical Research Council (grant no. MR/V037315/1), Cystic Fibrosis Trust (grant no. SRC015) and Department of Health and Social Care (DHSC) Centre for Antimicrobial Optimisation (CAMO), Imperial College London. AL and DAJ hold funding from MRC CARP funding MR/V037315/

AUTHOR CONTRIBUTIONS

A.A., T.W., and X.S. designed and performed experiments, analyzed data, and wrote the article. D.A-J, B.L., and A.R. designed the study and experiments, analyzed data, and critically reviewed the article.

DECLARATION OF INTERESTS

D.A-J. holds share options in Pulmocide Ltd. A.R. receives consultancy fees from Pulmocide. The authors declare no competing interests.

STAR★METHODS

Detailed methods are provided in the online version of this paper and include the following:

- KEY RESOURCES TABLE
- EXPERIMENTAL MODEL AND STUDY PARTICIPANT DETAILS
  - Human cells
  - Fungal strains
- METHOD DETAILS
  - Isolation and culture of human myeloid cells
  - Aspergillus fumigatus strains and culture
  - Imaging flow cytometry (Imagestream X)
  - Colony forming unit (CFU) assay
  - cDNA generation and real-time thermal cycling
  - Myeloid cell/CD4 T cell co-culture and T cell colorimetric proliferation ELISA
  - T cell proliferation assay
  - Enzyme-linked immunosorbent assays (ELISAs)
  - RNA isolation for next generation sequencing
  - RNA-seq library prep
  - Adapter ligation
  - DNA fragment enrichment
  - Library validation, normalisation and sequencing
  - ChIP-seq
  - Cross-linking
  - DNA fragmentation
  - Chromatin immunoprecipitation
  - DNA de-crosslinking
  - DNA purification
  - DNA quantification
  - ChIP-PCR validation
  - ChIP-seq library prep
- QUANTIFICATION AND STATISTICAL ANALYSIS

SUPPLEMENTAL INFORMATION

Supplemental information can be found online at https://doi.org/10.1016/j.isci.2024.111535.

Received: May 20, 2024
Revised: August 11, 2024
Accepted: December 3, 2024
Published: December 6, 2024

REFERENCES

1. Khush, K.K., Cherikh, W.S., Chambers, D.C., Goldfarb, S., Hayes, D., Jr., Kucheryavaya, A.Y., Levvey, B.J., Meiser, B., Rossano, J.W., and Stehlik, J.; International Society for Heart and Lung Transplantation (2018). The International Thoracic Organ Transplant Registry of the International

Society for Heart and Lung Transplantation: Thirty-fifth Adult Heart Transplantation Report-2018; Focus Theme: Multiorgan Transplantation. J. Heart Lung Transplant. *37*, 1155–1168.

2. Pappas, P.G., Alexander, B.D., Andes, D.R., Hadley, S., Kauffman, C.A., Freifeld, A., Anaissie, E.J., Brumble, L.M., Herwaldt, L., Ito, J., et al. (2010). Invasive fungal infections among organ transplant recipients: results of the Transplant-Associated Infection Surveillance Network (TRANSNET). Clin. Infect. Dis. *50*, 1101–1111. https://doi.org/10.1086/651262.
3. Iversen, M., Burton, C.M., Vand, S., Skovfoged, L., Carlsen, J., Milman, N., Andersen, C.B., Rasmussen, M., and Tvede, M. (2007). Aspergillus infection in lung transplant patients: incidence and prognosis. Eur. J. Clin. Microbiol. Infect. Dis. *26*, 879–886. https://doi.org/10.1007/s10096-007-0376-3.
4. Remund, K.F., Best, M., and Egan, J.J. (2009). Infections relevant to lung transplantation. Proc. Am. Thorac. Soc. *6*, 94–100. https://doi.org/10.1513/pats.200809-113GO.
5. Scheffert, J.L., and Raza, K. (2014). Immunosuppression in lung transplantation. J. Thorac. Dis. *6*, 1039–1053. https://doi.org/10.3978/j.issn.2072-1439.2014.04.23.
6. Treede, H., Glanville, A.R., Klepetko, W., Aboyoun, C., Vettorazzi, E., Lama, R., Bravo, C., Knoop, C., Aubert, J.D., and Reichenspurner, H.; European and Australian Investigators in Lung Transplantation (2012). Tacrolimus and cyclosporine have differential effects on the risk of development of bronchiolitis obliterans syndrome: results of a prospective, randomized international trial in lung transplantation. J. Heart Lung Transplant. *31*, 797–804. https://doi.org/10.1016/j.healun.2012.03.008.
7. Neurohr, C., Huppmann, P., Zimmermann, G., Leuchte, H., Baumgartner, R., Hatz, R., Frey, L., Uberfuhr, P., Bittmann, I., Behr, J., et al. (2009). Tacrolimus and mycophenolate mofetil as first line immunosuppression after lung transplantation. Transpl. Int. *22*, 635–643. https://doi.org/10.1111/j.1432-2277.2009.00843.x.
8. Hachem, R.R., Yusen, R.D., Chakinala, M.M., Meyers, B.F., Lynch, J.P., Aloush, A.A., Patterson, G.A., and Trulock, E.P. (2007). A randomized controlled trial of tacrolimus versus cyclosporine after lung transplantation. J. Heart Lung Transplant. *26*, 1012–1018.
9. Herbst, S., Shah, A., Carby, M., Chusney, G., Kikkeri, N., Dorling, A., Bignell, E., Shaunak, S., and Armstrong-James, D. (2013). A new and clinically relevant murine model of solid-organ transplant aspergillosis. Dis. Model. Mech. *6*, 643–651. https://doi.org/10.1242/dmm.010330.
10. Ramirez-Ortiz, Z.G., and Means, T.K. (2012). The role of dendritic cells in the innate recognition of pathogenic fungi (A. fumigatus, C. neoformans and C. albicans). Virulence *3*, 635–646. https://doi.org/10.4161/viru.22295.
11. Mezger, M., Kneitz, S., Wozniok, I., Kurzai, O., Einsele, H., and Loeffler, J. (2008). Proinflammatory response of immature human dendritic cells is mediated by dectin-1 after exposure to Aspergillus fumigatus germ tubes. J. Infect. Dis. *197*, 924–931. https://doi.org/10.1086/528694.
12. Park, S.J., Burdick, M.D., and Mehrad, B. (2012). Neutrophils mediate maturation and efflux of lung dendritic cells in response to Aspergillus fumigatus germ tubes. Infect. Immun. *80*, 1759–1765. https://doi.org/10.1128/IAI.00097-12.
13. Bozza, S., Gaziano, R., Spreca, A., Bacci, A., Montagnoli, C., di Francesco, P., and Romani, L. (2002). Dendritic cells transport conidia and hyphae of Aspergillus fumigatus from the airways to the draining lymph nodes and initiate disparate Th responses to the fungus. J. Immunol. *168*, 1362–1371. https://doi.org/10.4049/jimmunol.168.3.1362.
14. Lamhamedi-Cherradi, S.E., Martin, R.E., Ito, T., Kheradmand, F., Corry, D.B., Liu, Y.J., and Moyle, M. (2008). Fungal proteases induce Th2 polarization through limited dendritic cell maturation and reduced production of IL-12. J. Immunol. *180*, 6000–6009.
15. Vukcevic, M., Zorzato, F., Spagnoli, G., and Treves, S. (2010). Frequent calcium oscillations lead to NFAT activation in human immature dendritic cells. J. Biol. Chem. *285*, 16003–16011. https://doi.org/10.1074/jbc.M109.066704.
16. Plantinga, M., Guilliams, M., Vanheerswynghels, M., Deswarte, K., Branco-Madeira, F., Toussaint, W., Vanhoutte, L., Neyt, K., Killeen, N., Malissen, B., et al. (2013). Conventional and monocyte-derived CD11b(+) dendritic cells initiate and maintain T helper 2 cell-mediated immunity to house dust mite allergen. Immunity *38*, 322–335. https://doi.org/10.1016/j.immuni.2012.10.016.
17. McWilliam, A.S., Napoli, S., Marsh, A.M., Pemper, F.L., Nelson, D.J., Pimm, C.L., Stumbles, P.A., Wells, T.N., and Holt, P.G. (1996). Dendritic cells are recruited into the airway epithelium during the inflammatory response to a broad spectrum of stimuli. J. Exp. Med. *184*, 2429–2432. https://doi.org/10.1084/jem.184.6.2429.
18. Zanoni, I., Ostuni, R., Capuano, G., Collini, M., Caccia, M., Ronchi, A.E., Rocchetti, M., Mingozzi, F., Foti, M., Chirico, G., et al. (2009). CD14 regulates the dendritic cell life cycle after LPS exposure through NFAT activation. Nature *460*, 264–268. https://doi.org/10.1038/nature08118.
19. Granucci, F., Zanoni, I., Pavelka, N., Van Dommelen, S.L.H., Andoniou, C.E., Belardelli, F., Degli Esposti, M.A., and Ricciardi-Castagnoli, P. (2004). A contribution of mouse dendritic cell-derived IL-2 for NK cell activation. J. Exp. Med. *200*, 287–295. https://doi.org/10.1084/jem.20040370.
20. Zanoni, I., Foti, M., Ricciardi-Castagnoli, P., and Granucci, F. (2005). TLR-dependent activation stimuli associated with Th1 responses confer NK cell stimulatory capacity to mouse dendritic cells. J. Immunol. *175*, 286–292.
21. Hogan, P.G., Chen, L., Nardone, J., and Rao, A. (2003). Transcriptional regulation by calcium, calcineurin, and NFAT. Genes Dev. *17*, 2205–2232. https://doi.org/10.1101/gad.1102703.
22. Shah, A., Kannambath, S., Herbst, S., Rogers, A., Soresi, S., Carby, M., Reed, A., Mostowy, S., Fisher, M.C., Shaunak, S., and Armstrong-James, D.P. (2016). Calcineurin Orchestrates Lateral Transfer of Aspergillus fumigatus during Macrophage Cell Death. Am. J. Respir. Crit. Care Med. *194*, 1127–1139. https://doi.org/10.1164/rccm.201601-0070OC.
23. Herbst, S., Shah, A., Mazon Moya, M., Marzola, V., Jensen, B., Reed, A., Birrell, M.A., Saijo, S., Mostowy, S., Shaunak, S., and Armstrong-James, D. (2015). Phagocytosis-dependent activation of a TLR9-BTK-calcineurin-NFAT pathway co-ordinates innate immunity to Aspergillus fumigatus. EMBO Mol. Med. *7*, 240–258. https://doi.org/10.15252/emmm.201404556.
24. Armstrong-James, D., Teo, I.A., Shrivastava, S., Petrou, M.A., Taube, D., Dorling, A., and Shaunak, S. (2010). Exogenous interferon-gamma immunotherapy for invasive fungal infections in kidney transplant patients. Am. J. Transplant. *10*, 1796–1803. https://doi.org/10.1111/j.1600-6143.2010.03094.x.
25. Delsing, C.E., Gresnigt, M.S., Leentjens, J., Preijers, F., Frager, F.A., Kox, M., Monneret, G., Venet, F., Bleeker-Rovers, C.P., van de Veerdonk, F.L., et al. (2014). Interferon-gamma as adjunctive immunotherapy for invasive fungal infections: a case series. BMC Infect. Dis. *14*, 166. https://doi.org/10.1186/1471-2334-14-166.
26. Kelleher, P., Goodsall, A., Mulgirigama, A., Kunst, H., Henderson, D.C., Wilson, R., Newman-Taylor, A., and Levin, M. (2006). Interferon-gamma therapy in two patients with progressive chronic pulmonary aspergillosis. Eur. Respir. J. *27*, 1307–1310.
27. Calo, E., and Wysocka, J. (2013). Modification of enhancer chromatin: what, how, and why? Mol. Cell *49*, 825–837. https://doi.org/10.1016/j.molcel.2013.01.038.
28. Williamson, I., Berlivet, S., Eskeland, R., Boyle, S., Illingworth, R.S., Paquette, D., Dostie, J., and Bickmore, W.A. (2014). Spatial genome organization: contrasting views from chromosome conformation capture and fluorescence in situ hybridization. Genes Dev. *28*, 2778–2791. https://doi.org/10.1101/gad.251694.114.
29. Eguiluz-Gracia, I., Schultz, H.H., Sikkeland, L.I., Danilova, E., Holm, A.M., Pronk, C.J., Agace, W.W., Iversen, M., Andersen, C., Jahnsen, F.L., et al. (2016). Long-term persistence of human donor alveolar macrophages in lung transplant recipients. Thorax *71*, 1006–1011. https://doi.org/10.1136/thoraxjnl-2016-208292.
30. Shepardson, K.M., Jhingran, A., Caffrey, A., Obar, J.J., Suratt, B.T., Berwin, B.L., Hohl, T.M., and Cramer, R.A. (2014). Myeloid derived hypoxia

inducible factor 1-alpha is required for protection against pulmonary Aspergillus fumigatus infection. PLoS Pathog. *10*, e1004378. https://doi.org/10.1371/journal.ppat.1004378.

31. Rius, J., Guma, M., Schachtrup, C., Akassoglou, K., Zinkernagel, A.S., Nizet, V., Johnson, R.S., Haddad, G.G., and Karin, M. (2008). NF-kappaB links innate immunity to the hypoxic response through transcriptional regulation of HIF-1alpha. Nature *453*, 807–811. https://doi.org/10.1038/nature06905.
32. Liu, Y.V., Hubbi, M.E., Pan, F., McDonald, K.R., Mansharamani, M., Cole, R.N., Liu, J.O., and Semenza, G.L. (2007). Calcineurin promotes hypoxia-inducible factor 1alpha expression by dephosphorylating RACK1 and blocking RACK1 dimerization. J. Biol. Chem. *282*, 37064–37073.
33. Bierne, H., Hamon, M., and Cossart, P. (2012). Epigenetics and bacterial infections. Cold Spring Harb. Perspect. Med. *2*, a010272. https://doi.org/10.1101/cshperspect.a010272.
34. Haberland, M., Montgomery, R.L., and Olson, E.N. (2009). The many roles of histone deacetylases in development and physiology: implications for disease and therapy. Nat. Rev. Genet. *10*, 32–42. https://doi.org/10.1038/nrg2485.
35. Karouzakis, E., Gay, R.E., Gay, S., and Neidhart, M. (2009). Epigenetic control in rheumatoid arthritis synovial fibroblasts. Nat. Rev. Rheumatol. *5*, 266–272. https://doi.org/10.1038/nrrheum.2009.55.
36. Drury, J.L., and Chung, W.O. (2015). DNA methylation differentially regulates cytokine secretion in gingival epithelia in response to bacterial challenges. Pathog. Dis. *73*, 1–6. https://doi.org/10.1093/femspd/ftu005.
37. Pacis, A., Tailleux, L., Morin, A.M., Lambourne, J., MacIsaac, J.L., Yotova, V., Dumaine, A., Danckaert, A., Luca, F., Grenier, J.C., et al. (2015). Bacterial infection remodels the DNA methylation landscape of human dendritic cells. Genome Res. *25*, 1801–1811. https://doi.org/10.1101/gr.192005.115.
38. Ifrim, D.C., Quintin, J., Meerstein-Kessel, L., Plantinga, T.S., Joosten, L.A.B., van der Meer, J.W.M., van de Veerdonk, F.L., and Netea, M.G. (2015). Defective trained immunity in patients with STAT-1-dependent chronic mucocutaneaous candidiasis. Clin. Exp. Immunol. *181*, 434–440. https://doi.org/10.1111/cei.12642.
39. Uze, G., Schreiber, G., Piehler, J., and Pellegrini, S. (2007). The receptor of the type I interferon family. Curr. Top. Microbiol. Immunol. *316*, 71–95. https://doi.org/10.1007/978-3-540-71329-6_5.

STAR★METHODS

KEY RESOURCES TABLE

REAGENT or RESOURCE	SOURCE	IDENTIFIER
Antibodies		
CD38 PE, Clone HB12e	Biolegend	Cat#305322; RRID:AB_314515
CD209 (DC-SIGN), Clone 9E9A8	Biolegend	Cat# 330110, RRID:AB_1236468
NFATc2, Clone 16A12A31	Biolegend	Cat# 658402, RRID:AB_2562881
H3K4me1 polyclonal antibody	Diagenode	Cat# C15410194, RRID:AB_2637078
H3K4me3 polyclonal antibody	Diagenode	Cat# C15410003, RRID:AB_2616052
H3K27ac polyclonal antibody	Diagenode	Cat# C15410196, RRID:AB_2637079
Bacterial and virus strains		
Aspergillus fumigatus - CEA10	Fungal Genetics Stock Center	FGSC# A1163
Biological samples		
Leukocyte cones	National blood transfusion service	NHSBT
Chemicals, peptides, and recombinant proteins		
Recombinant GM-CSF	R&D Systems	Cat# 215-GM-010/CF
Recombinant IL-4	Peprotech	Cat# 200-04-20UG
Tacrolimus (FK506)	Selleckchem	Cat# S5003
Recombinant Human Interferon-γ (hIFN-γ)	Cell Signaling	Cat# 80385
Calcofluor White Stain	Merck	Cat# 18909
TRI Reagent® (Trizol)	Merck	Cat# T9424
Critical commercial assays		
Pan Monocyte Isolation Kit, human	Miltenyi Biotec	Cat# 130-096-537
$CD4^+$ T cell Isolation Kit, human	Miltenyi Biotec	Cat# 130-096-533
Human TNFa ELISA Kit	R&D Systems	Cat# DY210
Human IL-2 ELISA Kit	R&D Systems	Cat# DY202
Human IL-10 ELISA Kit	R&D Systems	Cat# DY217B
Human IL-12 ELISA Kit	R&D Systems	Cat# DY1270
BrdU Assay	Roche	Cat# 11647229001
Agilent High Sensitivity DNA Kit	Agilent	Cat# 5067-4626
Quant-iT dsDNA HS Assay Kit, High Sensitivity	Invitrogen	Cat# Q33120
QuantiTect Reverse Transcription Kit	Qiagen	Cat# 205311
Agilent RNA 6000 Nano Kit	Agilent	Cat# 5067-1511
miRNeasy Mini Kit	Qiagen	Cat# 217004
iDeal ChIP-seq kit for Histones	Diagenode	Cat# C01010051
MicroPlex Library Preparation Kit	Diagenode	Cat# C05010012
IPure kit v2	Diagenode	Cat# C03010015
Deposited data		
RNAseq Raw Data	This Paper	Sequence Read Archive: PRJNA1053273
CHIPsew Raw Data	This Paper	Sequence Read Archive: PRJNA1053273
Oligonucleotides		
RCAN1 Fwd 5′-AGAAAGCAAGATGCATTTTAGAAAC-3′		
RCAN1 Rev 5′-CGCTGAAGATATCACTGTTTGC-3′		

(*Continued on next page*)

Continued

REAGENT or RESOURCE	SOURCE	IDENTIFIER
Software and algorithms		
Prism software (version 8.0)	GraphPad	
STAR: ultrafast universal RNA-seq aligner	https://doi.org/10.1093/bioinformatics/bts635	
The Sequence Alignment/Map format and SAMtools	https://doi.org/10.1093/bioinformatics/btp352	
Ultrafast and memory-efficient alignment of short DNA sequences to the human genome	https://doi.org/10.1186/gb-2009-10-3-r25	
Model-based analysis of ChIP-Seq (MACS)	https://doi.org/10.1186/gb-2008-9-9-r137	
Diffbind R/Bioconductor package version 2.8.0	https://doi.org/10.1038/nature10730	
LOLA: enrichment analysis for genomic region sets and regulatory elements in R and Bioconductor	https://doi.org/10.1093/bioinformatics/btv612	
MEME SUITE: tools for motif discovery and searching	https://doi.org/10.1093/nar/gkp335	
Integrative Genomics Viewer (IGV): high-performance genomics data visualization and exploration	https://doi.org/10.1093/bib/bbs017	
Other		
RPMI-1640 media	Sigma-Aldrich	Cat# R8758
FBS	Sigma-Aldrich	Cat# F9665
Penicillin-Streptomycin	Gibco	Cat# 15140122
Ficoll-Paque™ PREMIUM	GE Healthcare	Cat# 17-5442-03
Sabouraud Dextrose Agar	Scientific Laboratory Supplies	Cat# cm041b
Miracloth	Merck	Cat# 475855-1R
FcR Blocking Reagent, human	Miltenyi Biotec	Cat# 130-059-901
JumpStart™ Taq ReadyMix™	Merck	Cat# P2893
SuperScript™ II Reverse Transcriptase	Thermofisher	Cat# 18064014
Beckman Coulter™ Agencourt AMPure XP	FisherSci	Cat# 10136224
Ethylenediaminetetraacetic acid	ThermoFisher	Cat# AM9260G
Bioruptor® Plus TPX microtubes	Diagenode	Cat# C30010010
qRT-PCR Brilliant III SYBR Master Mix	Agilent	Cat# 600886

EXPERIMENTAL MODEL AND STUDY PARTICIPANT DETAILS

Human cells

Cells used in this study were taken from bronchoalveolar lavage fluid from lung transplant patients undergoing bronchoscopy at Harefield Hospital or from leukocyte cones provided by the NHS Blood and Transfusion Service. Clinical information for patients is shown in Table 1.

The study was approved by the Biomedical Research Unit Biobank research project (Advanced lung disease, NRES reference, 10/H0504/9), Royal Brompton and Harefield NHS Trust. All experimentation was in line with the World Medical Association Declaration of Helsinki principles and the 1978 Belmont Report of US Department of Health & Human Services.

Fungal strains

Aspergillus fumigatus strain CEA10 (Fungal Genetics Stock Center, A1163) was utilised in this study.

METHOD DETAILS

Isolation and culture of human myeloid cells

Human monocytes were isolated by gradient centrifugation using Ficoll-Paque (GE Healthcare, UK) and enrichment through negative selection using a pan-monocyte isolation kit (Miltenyi Biotech, Auburn, CA). For monocyte derived macrophages (MDMs), monocytes were differentiated using 5 ng/ml GM-CSF (R&D, Abingdon, UK). For dendritic cell (DC) differentiation, GM-CSF at 25 ng/ml and IL-4 at 10 ng/ml was additionally used.

For isolation of CD4 T cells from peripheral blood, fresh autologous CD4 T cells were isolated 7 days after the monocyte isolation. CD4 T cells were enriched by negative selection using a CD4 T cell isolation kit (Miltenyi Biotec) according to the manufacturer's instructions. Purity was confirmed at >94%.

Treatment with FK506 (Prograf, Astellas; 25 ng/ml) was timed 1 h pre-inoculation on day 7 followed by interferon-γ 1000iu/ml (Cell Signaling) as appropriate.

Aspergillus fumigatus strains and culture

A. fumigatus CEA10 conidia were cultured on Sabaroud-Dextrose agar (Oxoid, Basingstoke, UK) for 3–5 days prior to harvest in 0.1% Tween and filtered through Miracloth (Calbiochem, UK). Conidia were swollen by incubating in RPMI 1640 medium (Sigma-Aldrich) at 1×10^6 conidia/ml at 37°C for 4 h. Conidia were centrifuged, resuspended, counted and diluted to the desired concentration. Where required, conidia were fixed in 2% paraformaldehyde in PBS for 10 min, washed in PBS, quenched in 0.1 M ammonium chloride for 10 min, and PBS-washed again.

Imaging flow cytometry (Imagestream X)

Relative numbers of dendritic cells and alveolar macrophages were enumerated from lung transplant recipient bronchoalveolar lavage fluid using CD1c (PerCPCy5.5, Clone: L161) as a marker for DCs and autofluorescence in the green channel was used as an indicator of alveolar macrophages.

DC or MDM were pre-treated with FK506 (10 ng/mL) for 1 h prior to infection with Calcofluor White (Sigma)-stained, live *A. fumigatus* SC (MOI = 1). Cells were detached, blocked using human Ig FcR Blocking Reagent (Miltenyi Biotec), and stained with for either CD83-PE (Clone HB15e) and DC-SIGN-PerCPCy5.5 (Clone 9E9A8) (Biolegend UK) or NFATc2-Cy5 (Clone.

16A12A31) (Biolegend UK) and DAPI. Samples were analyzed on Imagestream X imaging flow cytometer (Amnis).

For phagocytosis assays, the percentage of DCs with internalised conidia was quantified according to Calcofluor White fluorescence within the cell. For cell surface marker staining, the per cell mean fluorescent intensity (MFI) was calculated and the median MFI of a sample quantified.

Colony forming unit (CFU) assay

Day 7 dendritic cells pre-treated with FK506 and/or IFNγ were infected with *A. fumigatus* SC at an MOI 1 for 6 h. Cells were then washed to remove extra-cellular conidia and lysed in 0.1% Tween 20/dH2O. Serial dilutions were plated onto Sabouraud dextrose agar (Oxoid) plates. Plates were incubated at 37°C overnight and CFUs were counted the next day.

cDNA generation and real-time thermal cycling

RNA extraction was performed using the phenol-chloroform method. Briefly, DCs were pre-treated with vehicle or FK506 for 1 h before stimulation with live *A. fumigatus* swollen conidia (MOI = 1). Samples were incubated in Trizol (Sigma-Aldrich) to lyse the cells then mixed with chloroform, RNA was precipitated by isopropanol (VWR) and washed twice with ice-cold 70% ethanol before eluting in nuclease-free water (Ambion). Sample RNA concentrations were determined on a NanoDrop 1000 Spectrophotometer (Thermo Scientific). cDNA was prepared using the QuantiTect Reverse Transcription kit (Qiagen) according to the manufacturer's instructions. RCAN1.4 expression was measured using the following primers: Forward primer 5′-AGAAAGCAAGATGCATTTTAGAAAC-3′, Reverse primer 5′-CGCTGAAGATATCACTGTTTGC-3'. mRNA expression was normalised to β-actin. Taqman quantitative PCR was carried out using JumpStart Taq Polymerase ReadyMix (Sigma-Aldrich) according to the manufacturer's instructions. The reaction was run on an ABI 7900 HT Fast Real-Time PCR machine (Applied Biosystems, Paisley, UK). Fold change of gene expression $2^{-\Delta\Delta Ct}$ method.

Myeloid cell/CD4 T cell co-culture and T cell colorimetric proliferation ELISA

Day 7 dendritic cells pre-treated with FK506 and/or IFNγ were infected with *A. fumigatus* SC at an MOI 1. After 1 h of infection, the treatments were washed off and autologous CD4 T cells were added to the culture. Cells were then incubated at 37°C 5% CO2 for a total of 12 h with addition of Day 7 MDM's at the 6-h mark where appropriate. A cell ratio of moDC: CD4 T cell 1:5 was used.

T cell proliferation assay

T cell proliferation was assessed using a using a 5-bromo-deoxyuridine (BrdU) assay (Roche) according to the manufacturer's instructions. Absorbance was measured with an iMarkTM Microplate reader at 370 nm (reference wavelength 492 nm) and normalized to background.

Enzyme-linked immunosorbent assays (ELISAs)

All ELISAs (TNFα, IL-2, IL-10, IL-12) were carried out using the human Duoset 'sandwich' ELISA kits (R&D Systems), according to manufacturers' protocols.

RNA isolation for next generation sequencing

RNA extraction was performed using the miRNeasy Mini spin column kit (Qiagen, Germany) according to the manufacturer's instructions, quantified on the NanoDrop 1000 Spectrophotometer (Thermo Scientific) and integrity assessed qith an RNA 6000 Nano chip

(Agilent, California) and a Bioanalyzer 2100 (Agilent). Samples with electropherograms showing high quality 18S and 28S peaks, flat baselines and composite RNA integrity scores (RIN) greater that 8 out of 10 were deemed suitable for RNA-Seq library preparation. This was confirmed by running formaldehyde 1% agarose gels with ethidium bromide staining of RNA.

RNA-seq library prep

RNA-seq libraries were prepared using the Truseq stranded mRNA sample preparation kit (Illumina, California) according to the manufacturer's instructions. Samples were resuspended with 8 μL of First Strand Synthesis Act D Mix (containing SuperScript II Reverse Transcriptase (Thermo Fisher) and First Strand Synthesis Act D Mix at a 1:9 ratio) then incubated on the thermal cycler.

For second strand cDNA synthesis the RNA template is removed and a replacement strand is synthesized incorporating dUTP in place of dTTP, which quenches the second strand during amplification as polymerase does not incorporate past this nucleotide, thus generating ds cDNA. After a 4°C hold, samples were resuspended with 20 μL of Second Strand Marking Master Mix and 5 μL of Resuspension Buffer and incubated at 16°C for 1 h, before incubating for 15 min at room temperature with 90 μL of AMPure XP beads (Beckman Coulter, California) to separate the ds cDNA from the reaction mix and placed on the magnetic stand, then supernatant discarded. After two 80% EtOH washes, samples were resuspended in 17.5 μL Resuspension Buffer. 15 μL of supernatant from each well, containing blunt-ended double stranded cDNA, was transferred to a new plate. The 3′ ends of the blunt fragments were adenylated with a single 'A' nucleotide prior to adapter ligation (which have a complementary overhanging single.

'T' nucleotide on the 3′ end to permit ligation) to prevent aberrant dimerization of fragments. 12.5 μL of A-Tailing Mix was added to each well, followed by incubation at 37°C for 30 min, 70°C for 5 min, then a 4°C hold.

Adapter ligation

Unique indexing adapters were ligated to the ends of the ds cDNA to barcode each sample within a pool. 2.5 μL of Ligation Control and 2.5 μL of Ligation Mix and 2.5 μL of the unique identifying RNA Adapter Index were added to each sample, followed by centrifugation at 280 × g for 1 min. Samples were incubated at 30°C for 10 min before the addition of 5 μL of Stop Ligation Buffer to inactivate the ligation. Samples were resuspended with 42 μL of mixed AMPure XP Beads and the plate incubated at room temperature for 15 min before transfer to the magnetic stand. 79.5 μL supernatant was discarded, and two 200 μL 80% EtOH washes were performed. Samples were permitted to air-dry for 15mins before resuspension in 52.5 μL of Resuspension Buffer. 50 μL supernatant from each well was transferred to a new plate, a further 50 μL AMPure XP Beads cleanup performed, followed by two further 200 μL 80% EtOH washes. After a further 15 min air-dry, beads were resuspended in 22.5 μL Resuspension Buffer, placed on the magnetic stand, and 20 μL supernatant (containing adapter-ligated cDNA) was transferred to a new PCR plate.

DNA fragment enrichment

PCR amplification of the adapter-ligated, indexed cDNA samples was performed to amplify the amount of DNA in the library. Fragments that failed to ligate adapters to both ends are selected out. 5 μL of thawed PCR Primer Cocktail (anneals to the ends of the adapters) and 25 μL of thawed PCR Master Mix were added to each well. The following cycling program, incorporating a deliberately reduced number of PCR cycles, was run:

After an AMPure XP Beads clean-up and two 200 μL 80% EtOH washes, the samples were air-dried at room temperature for 15 min on the magnetic stand, before resuspending in 32.5 μL Resuspension Buffer. 30 μL of supernatant from each well, containing the final library of PCR-amplified indexed cDNA was transferred to a storage plate.

Library validation, normalisation and sequencing

One μL of each cDNA library was loaded onto a High-Sensitivity DNA chip (Agilent) and analyzed on the Bioanalyzer 2100 (Agilent). Median average fragment size per sample was 320 bp (IQR: 306–335). Final sample concentration was corroborated with a Qubit fluorometer using the Quant-iT dsDNA HS Assay Kit (Thermo Fisher). Samples were normalized to the lowest concentration cDNA sample and an equal amount of cDNA from each uniquely indexed sample was added to a pool. Each pool, with a maximum 8 samples, was analyzed at the MRC LMS Bioinformatics core facility by paired-end sequencing on a HiSeq 2500 sequencer (Illumina).

ChIP-seq

Chromatin immunoprecipitation was performed using the iDeal ChIP-Seq kit for Histones, and the Microplex Library preparation kit (Diagenode).

Cross-linking

MoDC's at $1x10^7$ per flask were pre-treated with FK506 and/or IFNγ and infected with swollen *A. fumigatus* conidia for 1 h. Flasks were pipetted-washed to harvest, with the aid of 10 min of cold 5 mM EDTA, and transferred to 1.5 mL Eppendorf tubes. Samples were fixed and DNA cross-linked by incubation with 1% formalin for 10 min at room temperature and the reaction stopped by the incubation with 1.25 mM glycine for 5 min. Samples were then washed in PBS twice then resuspended in lysis buffer.

DNA fragmentation

DNA was fragmented by sonication of 200 μL volumes of samples in 1.5 mL TPX sonication tubes (Diagenode) and placed in the Bioruptor Sonication System (Diagenode) for 30 cycles of 30s on/30s off at high power. A small fraction (2–5%) of each sample was set aside as input DNA. Post-fragmentation, an agarose gel was run to assess sonication efficiency.

Chromatin immunoprecipitation

Target antibodies used were rabbit anti-human polyclonal H3K4me1 (pAb-194-050), H3K4me3 (pAb-003-050) and H3K27ac (pAb-196-050, all Diagenode). H3K4me3 or H3K4me1 respectively and Rabbit IgG served as positive and negative control antibodies for the experiments. Fragmented samples were incubated overnight on a rotating wheel at 40 rpm at 4°C with Protein-A-coated magnetic beads, 5% BSA and protease inhibitors with a pre-optimised amount of the appropriate antibody (1 μg for H3K4me1 or H3K27ac, 1.5 μg for H3K4me3). Samples were assessed for quality on the Bioanalyzer 2100 (Agilent) and for quantity on the Qubit 2.0 Fluorometer (Invitrogen).

DNA de-crosslinking

After four buffer washes in a magnetic rack, immunoprecipitated samples were eluted in SDS/NaHCO3 buffer and, along with input DNA samples, were incubated at 65°C in a heat block for 4 h to reverse the crosslinks.

DNA purification

The de-cross-linked samples were mixed with 100% isopropanol then magnetic IPure V2, beads (Diagenode), followed by washes with IPOH-containing wash buffer to purify the DNA, prior to elution from the beads with Elution buffer C (Diagenode).

DNA quantification

Post-ChIP and input DNA samples were quantified using the Qubit 2.0 fluorometer (Invitrogen) using the Qubit ds DNA HS kit with standards.

ChIP-PCR validation

To validate the immunoprecipitation, RT-PCR was performed of the positive and negative control antibodies to a known positive and negative control loci of the positive control antibody. Primer pairs for the GADPH promoter (positive locus) and Myoglobin exon 2 (negative locus) were targets for H3K4me3 when used as a positive control Ab, and GAS2L1 region (positive locus) and GAPDH promoter (negative locus) were targets for H3K4me1 when used as positive control Ab.

For each PCR reaction a 10ul volume was analyzed, comprising 5ul of 2x Brilliant III Ultra-Fast SYBR Green QPCR Master Mix (Agilent), 2ul of sample, 1ul of primer pair and 1ul of nuclease-free water. Reactions were run on the ABI 7900 HT Fast Real-Time PCR machine (Applied Biosystems, Paisley, UK) using the following cycling program: - Percentage recovery was measured as 2^(Ctinput-Ctsample). Samples were deemed suitable for library preparation if the positive control target recovery was at least 5%, positive control target recovery was at most 1%, and the ratio of the two was greater than 5:1.

ChIP-seq library prep

dsDNA repair

Ten microliters of the immunoprecipitated sample of the input DNA was added to template preparation enzyme for DNA and incubated at 22°C for 25 min then 50°C for 20 min on a plate thermal cycler.

Adapter ligation

A library synthesis master-mix containing patent stem-loop adapters was added to the reaction then incubated at 22°C for 40 min.

Library amplification

Library amplification enzyme along with a corresponding unique indexing reagent was added to each reaction mix and the following program was set on the thermal cycler.

The number of amplification cycles was pre-optimised by real-time amplification of varying amounts of test DNA, and this was used to guide the appropriate number of cycles for each sample in the reaction, based on the starting quantity of DNA.

Library quality/quantity assessment, washing and pooling

As detailed for RNA-Seq above, samples were loaded onto the High-Sensitivity DNA assay chip and analyzed on the Bioanalyzer 2100 (Agilent). Electropherograms demonstrated smears peaking around 200-250 bp in length with minimal adapter contamination. A subsequent wash was done on each sample to eliminate smaller size fragment (Including adapter dimers) by re-suspending with an equivalent volume of Ampure beads, washing with 80% ethanol, and eluting in NFW. Post-wash quantification of each sample was done with a Qubit 2.0 fluorometer using the Quant-iT dsDNA HS Assay Kit. Samples were then normalized in volume to the lowest quantity sample and combined into pools of 6 samples for sequencing.

Sequencing

Each pool of 6 samples was single-end sequenced on one lane on the HiSeq 2500 sequencer (Illumina) using the standard protocol.

Computational processing of sequenced data

All analyses were performed using the Unix-like CLI Terminal on Mac OS, with secure shell to the Imperial ICT high performance computer ax3/4, using R/Bioconductor packages and are detailed in the individual chapters.

Quality control of raw sequenced files

All raw sequenced files were assessed for quality using FastQC version 0.11.3 (Babraham Institute Bioinformatics). Sequences were generally of high quality with no evidence of PCR over amplification i.e., sequence duplication levels fell well within pre-set acceptable limits (non-unique sequences less than 20% of the total). Where there was evidence of adapter contamination, detected by a high proportion of over-represented sequences, abnormal per sequence GC content or presence of known Illumina adapters, the sequences were trimmed and adapters removed using Trim Galore! version 0.4.0 (Babraham Institute Bioinformatics).

Alignment of RNA-sequenced reads to the reference genome

Reads were then aligned to the hg38 version of the human genome (downloaded from the USCS genome browser; https://genome.ucsc.edu) using the STAR: ultrafast universal RNA-seq aligner version 2.6 with the output received in BAM file format. BAM files were then ordered positionally based on their genomic alignment coordinates using Samtools version 1.2.1.

Differential gene expression

Using the edgeR R/Bioconductor package, the library size and a normalisation factor of each sample was calculated and thus the whole dataset was normalised by multiplying by a scaling factor. Then edgeR was used fit a negative binomial generalized log-linear model to the read counts for each gene. Differential gene expression was calculated by a Gene-Wise Likelihood Ratio Test to obtain *p*-values.

Gene Ontology analysis

Gene Ontology (GO) term enrichment analysis was performed for genes implicit in immune function compared to all genes present in the merged dataset. The clusterProfiler R/Bioconductor package (version 3.7) was used to perform enrichment analysis, and *p*-values were corrected for multiple testing using the Benjamini-Hochberg method.

Alignment of ChIP-sequenced reads to the reference genome

Reads were then aligned to the hg38 version of the human genome (downloaded form the USCS genome browser; https://genome.ucsc.edu) using bowtie2 version 2.3.0 with the output received in SAM file format. Samtools was used to merge the two paired-end reads.

Peak calling and differential binding analysis

Peaks were called using MACS version 1.4.2, with subtraction of the input (negative) control to derive true signal. The Diffbind R/Bioconductor package version 2.8.0 was used call differentially-bound peaks between two conditions. Enrichment analysis of genomic regions overlapping with ChIP-Seq-defined epigenetic marks was performed with the LOLA R/Bioconductor package version 1.10. The enrichment of sequence motifs at defined genomic regions was analyzed using MEME version 4.9.0.

Data visualization

Post-alignment BAM files were converted to TDF files for viewing using the igvtools function on the Integrative Genome Viewer.

QUANTIFICATION AND STATISTICAL ANALYSIS

All data are expressed as mean ± SEM. Statistics were calculated using Prism software (version 7.0; GraphPad) using one-way ANOVA (comparison of $\geq$3 groups), two-way ANOVA and Student's t test (comparison between 2 groups) were carried out. For all figures, *p* values are represented as follows: $^{*}p < 0.05$; $^{**}p < 0.01$; $^{***}p < 0.001$.